J. Fluid Mech. (2002), *vol.* 456, *pp.* 113–135.
DOI: 10.1017/S0022112001007480 Printed in the United Kingdom

Experimental and theoretical analysis of the wave decay along a long array of vertical cylinders

By H. KAGEMOTO[1], M. MURAI[2], M. SAITO[1], B. MOLIN[3] AND Š. MALENICA[4]

[1]Department of Environmental Studies, Graduate School of Frontier Sciences, The University of Tokyo, 7-3-1 Hongo, Bunkyo-ku, Tokyo 113-0033, Japan

[2]Faculty of Environment and Information Sciences, Yokohama National University, 79-7 Tokiwadai, Hodogaya-ku, Yokohama 240-8501, Japan

[3]Ecole Supérieure d'Ingénieurs de Marseille, 13451 Marseille cedex 20, France

[4]Bureau Veritas, 17bis Place des Reflets, la Défense 2, 92400 Courbevoie, France

(Received 19 March 2001 and in revised form 9 July 2001)

A row of fifty identical, truncated vertical cylinders is submitted to regular head waves, with wave periods in a narrow range around the period of the so-called Neumann trapped mode. The free-surface elevation is measured at 14 locations along the array. Response amplitude operators of the free-surface motion are compared with numerical predictions from a potential flow model. Resonance effects, at wave periods equal to or larger than the critical one, are found to be much less than given by the numerical model. It is advocated that these discrepancies are due to dissipative effects taking place in the boundary layers at the cylinder walls. An artificial means is devised to incorporate dissipation in the potential flow model, whereby the cylinder walls are made slightly porous; the inward normal velocity of the flow is related to the dynamic pressure. The coefficient of proportionality is based on existing knowledge for circular cylinders in oscillatory flows. With this modification in the numerical code, excellent agreement is obtained with the experiments. The numerical model is further used for the case of a very long array composed of 1000 cylinders; it is found that with dissipation at the cylinder walls, the wave action steadily decreases along the array, even for wave periods substantially larger than the critical one. On the other hand, at wave periods less than the critical one, dissipation plays a negligible role; the observed decay is solely due to diffraction effects. Implications of these results for very large structures such as column-supported floating airports are discussed. In particular, it is concluded that scale effects may be an important issue in the experimental analysis of such multi-column structures.

1. Introduction

In 1997 Maniar & Newman showed, through numerical computations, that resonant effects can take place when regular wave systems interact with long cylinder arrays, leading to large amplifications of the free-surface elevation and hydrodynamic loads, as compared to the single cylinder case. These results were obtained within the frame of linearized potential flow theory.

The main relevant parameters for these resonant phenomena to occur are the cylinder spacing to wavelength ratio and, to a lesser extent, the cylinder radius to spacing ratio. They are usually expressed as $k_0 d$ and a/d, where k_0 is the wavenumber

($k_0 = 2\pi/L$, L being the wavelength), $2d$ the cylinder spacing (axis to axis), and a the radius.

The first resonant region occurs when $k_0 d$ is slightly less than $\frac{1}{2}\pi$ (meaning a wavelength slightly larger than twice the cylinder spacing). Maniar & Newman (1997) refer to this as the Neumann trapped mode case, with reference to Callan, Linton & Evans (1991) who showed that for a single cylinder between two parallel walls there exists a trapped mode at a neighbouring $k_0 d$ value; as the number of cylinders in the array increases to infinity, the two geometries become equivalent (one single cylinder in a channel or an infinite row of equally spaced cylinders).

Further, Maniar & Newman (1997) discovered other resonant regions, for $k_0 d$ values around π (the Dirichlet trapped mode) and at higher $k_0 d$ values (near-trapped modes).

From a practical viewpoint, these strikingly large water-surface elevations or wave loads could be a serious problem for a floating structure supported by a large number of vertical cylinders, such as is now being studied in Japan as a possible alternative to a land-based airport. In order to investigate what really happens in practice, comprehensive experiments are conducted in a wave tank. An array of 50 identical cylinders is submitted to regular waves with associated periods in the Neumann trapped mode range (the Dirichlet trapped mode and other near-trapped modes are of lesser concern since they occur at shorter wavelengths where the wave energy is reduced). The measured elevations, in-between the successive cylinders, are compared with calculated results from a potential flow code originally developed by Kagemoto & Yue (1986) and further improved by Murai, Kagemoto & Fujino (2000). In the resonant region, it is found that the measured elevations are much lower than the calculated ones.

It is argued that these discrepancies are due to dissipative effects taking place in the boundary layers at the cylinder walls. Since such viscous effects are difficult to accommodate within a potential flow model, an artificial means is employed that permits the dissipation of a controllable amount of energy at the solid boundaries; it consists in making them slightly porous, by relating the normal flow velocity to the hydrodynamic pressure. The choice of the coefficient of proportionality is made by reference to the two-dimensional case of a fixed cylinder in low-K_C oscillatory flow, first studied theoretically by Stokes (1851) and then experimentally by numerous investigators (e.g. Sarpkaya 1986; Troesch & Kim 1991; Bearman & Russell 1996).

The porous wall modification is easy to implement in the numerical model, or in a quasi-analytical method such as proposed by Linton & Evans (1990), which is used for validation. It is then found that the calculated elevations are in very good agreement with the measured ones.

Numerical results are then presented for a very long array consisting of 1000 cylinders, with and without energy dissipation, and for a rectangular system of 16×80 cylinders. The implications for full-scale structures are discussed.

2. Experimental campaign

2.1. *Set-up*

Fifty identical vertical truncated cylinders were fixed at equal distances in a water tank, as shown in figure 1. The horizontal dimensions of the tank are 50 m $\times$ 30 m and the water depth at the time of the experiments was 2.2 m. The diameter of the cylinders was 0.165 m and their draught 0.215 m. This may look a shallow draught

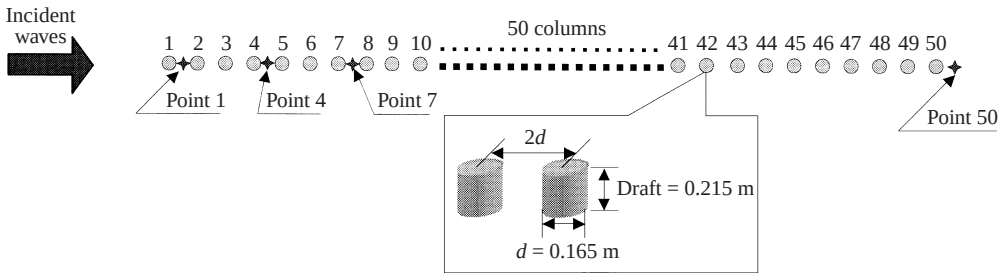

FIGURE 1. Geometry of the array of 1×50 cylinders.

but, at wave periods around 0.7 s, the wave action is much decreased at the foot of the cylinders (by a factor close to 6) and the finite draught effects are quite limited, as will be made clear later in the text.

They were arrayed in head waves, as shown in figure 1, and the centre-to-centre distance ($2d$) between adjacent cylinders was set to be 0.330 m (twice the diameter) for all the cylinders. This means an a/d ratio of 0.5. Each cylinder was fixed to a large steel bar via a rigid pipe so that the wave-induced oscillations of the cylinders were constrained. The distance between the cylinders was carefully adjusted by use of a specially constructed gauge. It was also checked that the axes of the cylinders were centred on a line drawn perpendicular to the wave-paddles on the bottom of the tank. The probable set-up error for the axis-to-axis distance between adjacent cylinders is estimated to be less than 0.5 mm while the probable lateral excursion of the cylinders from the line perpendicular to the wave-paddles is estimated to be less than 1 mm. The free-surface elevations among the cylinders were measured by capacitance-type wave probes at 14 locations, along the centreline of the array at exactly the same distance from the nearest two cylinders. The specific locations of the wave probes are 1-2, 4-5, 7-8, 10-11, 13-14, 16-17, 19-20, 22-23, 26-27, 30-31, 34-35, 38-39, 46-47, 50-51, where i-$(i+1)$ indicates that the corresponding wave probe was located right in-between the ith cylinder and the $(i+1)$th cylinder, counted from the head of the array. The expected maximum error of the measured surface elevations estimated from the calibrations of the wave probes is less than 0.5 mm. As will be described below, incident regular waves of three different wave heights (double amplitudes), 1 cm, 2 cm, 3 cm, were used in the experiments. Strict care was taken that the actual waveheight was within the allowable difference ($\pm 10\%$) from its prescribed value. Furthermore, the experiments were conducted with time intervals of more than 30 min so that the water surface in the tank was completely calm before the wavemaker was initiated.

2.2. *Results and comparisons with linearized potential flow theory*

Figure 2 shows the response amplitude operators (RAOs) of the vertical motion of the free surface, at the 14 gauges along the array, in regular waves of 2 cm waveheight and of periods 0.60, 0.65, 0.68, 0.69, 0.70, 0.71, 0.72 and 0.75 s. The RAOs were derived through Fourier analysis of the measured records. They are compared with calculated values, using the numerical model described in Murai *et al.* (2000). All tests were duplicated or in some cases triplicated, so their results appear as '1st', '2nd' and '3rd' in the figures.

According to Maniar & Newman (1997), for a radius to half-spacing a/d ratio of 0.5, and for 50 cylinders, the maximum amplification is attained for $k_0 d = 1.388911$ (their table 3), that is, in our experiments, a wave period of 0.6914 s. In this wave

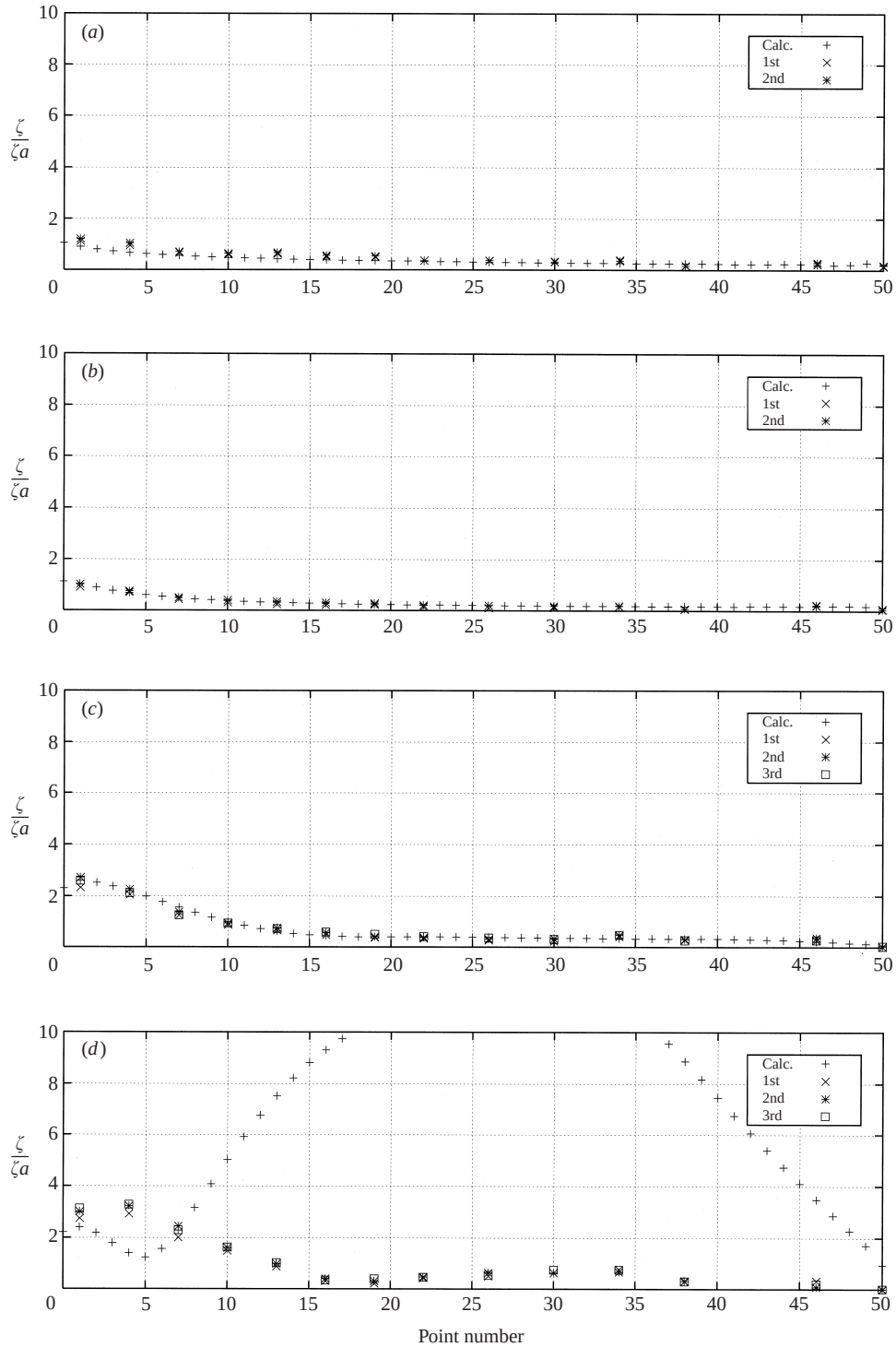

FIGURE 2. For caption see facing page.

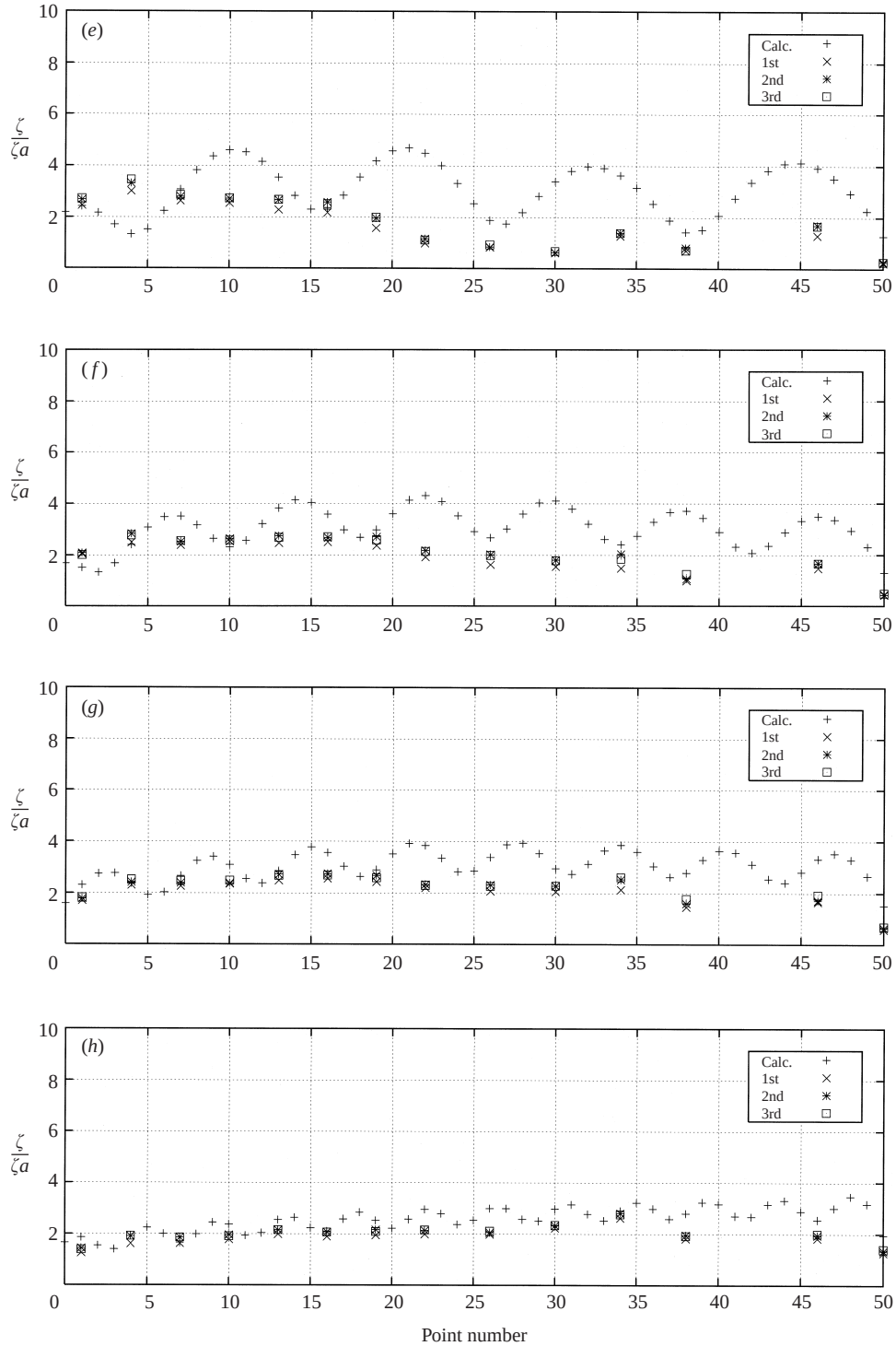

FIGURE 2. Response amplitude operators of the free-surface motion along the array. Measured *vs.* calculated values. Waveheight 2 cm. Wave period (*a*) 0.60 s; (*b*) 0.65 s; (*c*) 0.68 s; (*d*) 0.69 s; (*e*) 0.70 s; (*f*) 0.71 s; (*g*) 0.72 s; (*h*) 0.75 s.

condition, the peak value of the RAO is attained in the middle of the array. In the same table, Maniar & Newman (1997) give the resonant k_0d values for arrays of 25 ($k_0d = 1.382053$) and 10 ($k_0d = 1.346352$) cylinders, that is, respectively, wave periods of 0.6931 and 0.7023 s. As written by Newman (1997), it can be inferred that, at a wave period of 0.6931 s, two modulations would be observed along the $50 = 2 \times 25$ cylinders array, whereas at 0.7023 s, five modulations would be seen.

Maniar & Newman's results refer to infinite draught cylinders, whereas ours are truncated at a draught of 0.215 m, that is, for wave periods around 0.7 s, about 30% of the wavelength. The bottoms of the cylinders are hardly reached by the wave action, which is reduced by a factor of about 6 as compared to its value at the free surface. It was checked numerically that practically identical results are obtained in either case (infinite draught or 0.215 m draught). This point is further commented on in § 4 (see figure 5(*a*)), where it is observed that the finite draught results in a very small shift of the resonant periods, of about −0.002 s.

As expected from Maniar & Newman's results, figure 2(*d*), at the wave period 0.69 s shows calculated RAOs far above 10 by the middle of the array. The experimental values do not exceed 3.5, at the head of the array, and they decay to less than 1 beyond the twelfth cylinder.

Similarly, figure 2(*e*), at the wave period 0.70 s, reveals about four modulations along the array for the calculated RAOs, with maximum values around 5. The experimental results do not exhibit these four modulations, and do not exceed 3 at the head of the array, while they decay to less than 2 at its rear part.

In figure 2(*f*), corresponding to a wave period of 0.71 s, about six modulations are given by the numerical computations, with peak RAO values around 4. Again the experimental results are much lower, with decaying values toward the end of the array. Similar results are obtained at the larger wave periods of 0.72 and 0.75 s; the measured elevations are markedly lower than the calculated ones at the rear part of the array.

On the other hand, very good agreements between numerical and experimental results are observed in figures 2(*a*)–2(*c*), where the wave periods are below the critical value 0.69 s. As observed by Maniar & Newman (1997), at these wave periods, diffraction effects result into a quick decay of the free-surface elevation along the array.

The experimental results shown in figures 2(*d*)–2(*h*) raise some questions with regard to their validity, such as: Has a steady state been attained? Haven't nonlinear effects, such as wave breaking, come into play? What about parasitic effects such as reflections from the sidewalls, or from the beach?

To answer the first question, we produce in figure 3 the time traces of the free-surface elevations, as measured at gauges 7, 13, 19, 26, 34 and 46, at the 0.70 s wave period. It can be seen that a steady state is attained, except by the end of the array where the increases in amplitude that occur after some time are due to reflection from the beach (which was not very efficient at such low wave periods). Experimental values as produced in the figures were extracted from the measured values at time instants between 60 and 80 s, when transients have died out and reflections from the beach have not arrived yet.

To answer the second question, tests have been replicated at wave heights of 1 and 3 cm. The free-surface RAOs obtained from the measurements are shown in figures 4(*a*)–4(*c*), which correspond to figures 2(*d*), 2(*e*) and 2(*g*). It can be observed that the experimental RAOs derived from the three wave heights coalesce into nearly the same points. Also, no wave breaking was observed visually during the tests. It

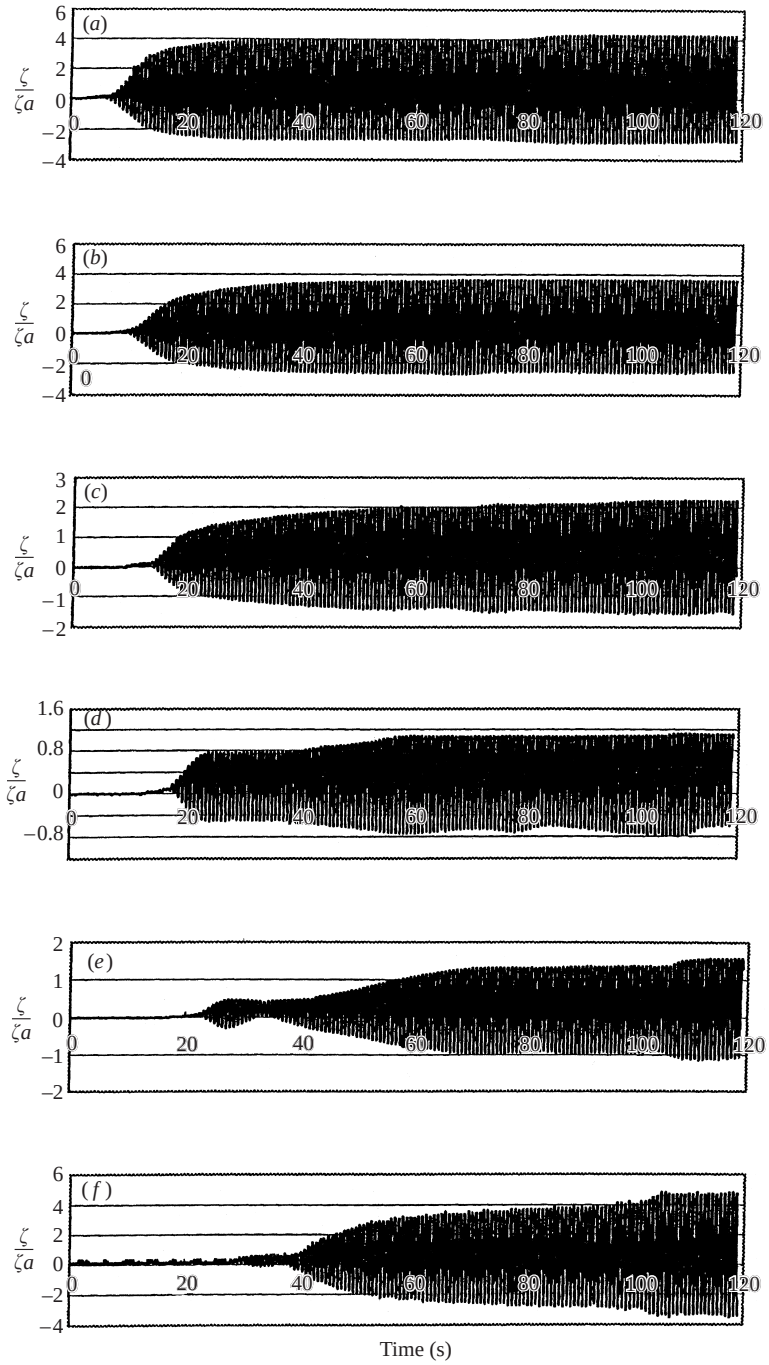

FIGURE 3. Time traces of the free-surface elevation at 6 gauges along the array. Wave period 0.70 s. Waveheight 2 cm. (*a*) point 7; (*b*) point 13; (*c*) point 19; (*d*) point 26; (*e*) point 34; (*f*) point 46.

can therefore be concluded that nonlinear effects are not present and that other explanations must be looked for to explain the discrepancies between calculations and measurements.

Because of the large width of the tank (30 m), sidewall effects are not believed to

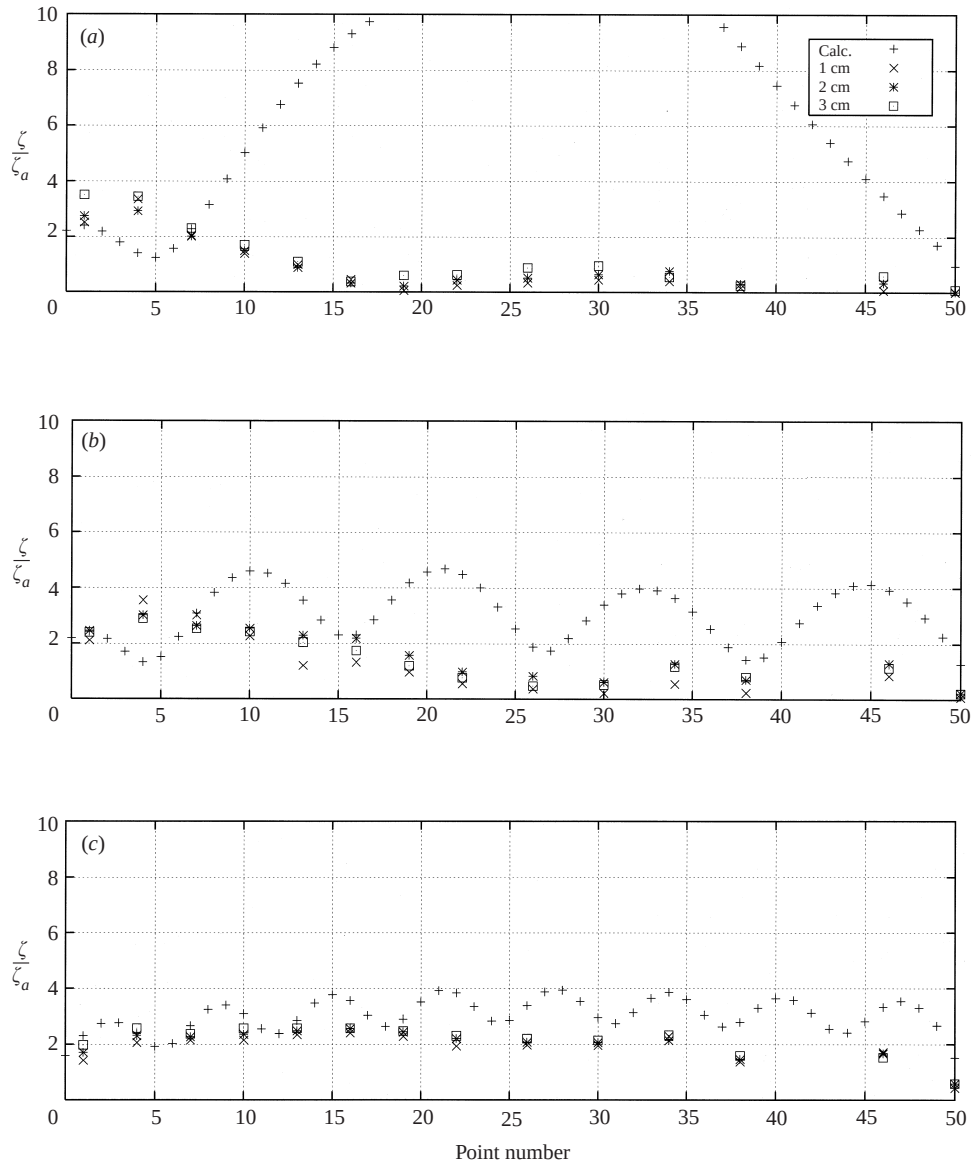

FIGURE 4. Calculated and measured RAOs of the free-surface elevation for three different waveheights. Wave period (*a*) 0.69 s; (*b*) 0.70 s; (*c*) 0.72 s.

be a relevant issue. The time taken for the diffracted waves to reflect off the walls and reach back to the array is about 55 s, at wave periods around 0.7 s. No evidence of such reflections can be seen on the time records.

Another possible explanation for the discrepancies would be that the cylinders are not perfectly aligned nor equally spaced. To investigate this point, calculations were performed where the cylinders are displaced from their reference positions by $\pm 5\%$ of their spacing, in the transverse and/or longitudinal directions. Nearly identical results were obtained.

As a result, it looked as if another explanation had to be found. What we may think of, when faced with such discrepancies between measured values and results from

potential flow calculations, is 'viscous effects'. This point is analysed in the following section.

3. Analysis of energy dissipation in the boundary layers

It is anticipated that the observed discrepancies, between measurements and numerical results, are due to viscous effects which are absent from the potential flow model.

To analyse these viscous effects we refer to the well-known and closely related problem of a two-dimensional circular cylinder in uniform oscillatory flow. This has received much attention, both through theory (Stokes 1851; Wang 1968; Hall 1984) and experiments (Honji 1981; Bearman *et al.* 1985; Sarpkaya 1986, to cite but a few).

For smooth cylinders, the flow is completely characterized by the Keulegan–Carpenter number K_C and by the Stokes parameter β, defined as

$$K_C = 2\pi\frac{A}{D}, \qquad \beta = \frac{D^2}{\nu T},$$

where D is the cylinder diameter, A the fluid motion amplitude away from the cylinder, ν the kinematic viscosity and T the oscillation period.

In the asymptotic limit when $K_C \to 0$ and $\beta \to \infty$, the theoretical solution, in the laminar regime, was given by Stokes in 1851. He found that, to the leading order in $\beta^{-1/2}$, the additional force due to viscosity is given by

$$F = \mathrm{Re}\left\{(1-\mathrm{i})\rho A\omega^2 D^2\sqrt{\frac{\pi}{\beta}}\mathrm{e}^{-\mathrm{i}\omega t}\right\} + O(\beta^{-1}), \tag{3.1}$$

the outer flow velocity being

$$U(t) = A\omega\cos\omega t.$$

When we rely upon the Morison equation to express the loading, this means a drag coefficient given by

$$C_D = \frac{3\pi^3}{2K_C}\frac{1}{\sqrt{\pi\beta}}, \tag{3.2}$$

while the added mass coefficient is slightly modified from its potential flow value:

$$C_m = 2 + \frac{4}{\sqrt{\pi\beta}}.$$

In our experiments, the cylinder diameter D is 16.5 cm and the critical wave period is 0.7 s, while the wave amplitude varies from 0.5 to 1.5 cm. Hence the β parameter is constant, $\beta \simeq 40\,000$, while K_C, based on the incident wave amplitude, goes from 0.19 to 0.57. The experiments give RAOs of the free-surface motion ranging from less than 1 up to 3 or 4, in resonant conditions. The practical K_C range, by the free surface, is therefore from 0.2 up to 2. At the feet of the cylinders, K_C values are much lower, but this is of no concern since most of the energy dissipation takes place close to the free surface (the amount of dissipated energy varies roughly as $\exp(2k_0 z)$ along the cylinder).

From reference experimental result, it can be stated that, at $\beta \simeq 40\,000$ and K_C between 0.2 and 2, the flow remains attached to the cylinder wall, but that the C_D values largely exceed the Stokes prediction.

For instance, Sarpkaya (1986) presents results for a circular cylinder in a U-tube

at $\beta = 11\,240$, K_C being as low as 0.8. For K_C less than 2.0, the measured drag coefficients turn out to be about 5 times as large as given by equation (3.2).

Other experimental results are given by Troesch & Kim (1991) who oscillate a circular cylinder in still water, at an oscillation frequency very close to the resonant frequency of the mechanical system. They present results at β values of 23 200 and 48 600, K_C ranging from 0.08 up to 0.5. They obtain results very similar to Sarpkaya's, that is, drag coefficients 4 to 5 times larger than the Stokes value over all the ranges of K_C. They conclude that the Stokes formula can still be used, provided the kinematic viscosity be replaced with an effective eddy viscosity, about 20 to 25 times as large.

Further, Bearman & Russell (1996) also present results from very careful experiments, at β numbers ranging from 20 000 up to 60 000. They conclude that the drag coefficient is approximated well by the simple formula

$$C_D = 2C_{D\text{Stokes}} + 0.08K_C$$

all over the investigated K_C range, from 0.1 up to 2. This means a C_D value about three times the Stokes prediction at $K_C \simeq 1.3$.

Why the C_D values obtained by Sarpkaya, Troesch & Kim, and Bearman & Russell do not quite agree is not clear. They all exceed the Stokes prediction, by a factors ranging from 2 to 5, even at very low K_C. It is known from theoretical analysis (Hall 1984) that at a critical K_C value given by $K_C^* = 5.778\beta^{-1/4}$ (that is $K_C^* \simeq 0.4$ in our case) three-dimensional instabilities appear in the boundary layers and result in the apparition of 'mushroom' vortices, first described by Honji (1981). However, observations show that Honji instabilities appear at much lower K_C values, from $K_C = 0.18$ at $\beta \simeq 40\,000$ (Sarpkaya 2001, personal communication).

In our case of a vertical cylinder in wave-induced flow, energy is also dissipated through frictional forces acting in the vertical direction, associated with the vertical component of the flow velocity. In the laminar regime, this can be estimated through the Stokes model of the oscillating flat plate (see e.g. Sarpkaya 1993 who considers the case of a long cylinder in oscillatory axial flow). Then we find that, at the k_0a values of our tests, the vertical friction forces dissipate about as much energy as the horizontal ones.

The combination of horizontal and vertical flow components at the cylinder wall should promote instabilities in the boundary layer (Sarpkaya 2001, personal communication). It can therefore be concluded that energy dissipation, in our experiments, by far exceeds the amount that can be estimated from the simple analysis based on the horizontal flow component, in the laminar regime. Whether it is 5 or 10 or 20 times larger is difficult to know. In the calculations described in the next section, somewhat arbitrarily, we have assumed a ratio of 10.

Another point of concern is that the cylinders are truncated and that, as a result, separation is likely to occur at their lower edges. Their draughts being 21.5 cm, at 0.7 s wave periods, the amplitude of the incoming wave flow motion at the cylinder keels is reduced by a factor of about 6, as compared to its free-surface-level value. Using drag coefficients such as given by Thiagarajan & Troesch (1994), it can be concluded that the magnitude of drag forces that result from flow separation is small, and that the energy dissipated through this effect is negligible as compared with the energy dissipated in the boundary layers (see the Appendix).

4. Modification of the numerical model

To render the effect of energy dissipation in the boundary layers, within our potential flow model, we use an indirect means whereby the cylinder walls are made

slightly 'porous'. Losses of head result from the fluid particles flowing in and out, which can be monitored to dissipate the proper amount of energy. Similar techniques are used in coastal and harbour engineering to simulate partly reflective boundaries.

The boundary condition at the cylinder walls is taken as

$$\frac{\partial \phi}{\partial R} = -\mathrm{i}\varepsilon \frac{\phi}{a}, \tag{4.1}$$

where a is the cylinder radius and the velocity potential $\Phi(x, y, z, t)$ is related to ϕ through

$$\Phi(x, y, z, t) = \mathrm{Re}\{\phi(x, y, z)\mathrm{e}^{-\mathrm{i}\omega t}\},$$

and ε is a small constant.

To determine realistic values for ε, we refer to the two-dimensional cylinder case, in harmonic flow. When the boundary condition (4.1) is taken at the wall, we readily obtain the velocity potential of the flow, to the leading order in ε, given by

$$\phi(R, \theta) = A\omega \cos\theta \left[R + (1 + 2\mathrm{i}\varepsilon)\frac{a^2}{R}\right] + O(\varepsilon^2), \tag{4.2}$$

and the hydrodynamic force on the cylinder is

$$F(t) = \mathrm{Re}\left\{-2\mathrm{i}\pi\rho a^2 A\omega^2(1 + 2\mathrm{i}\varepsilon)\mathrm{e}^{-\mathrm{i}\omega t}\right\}. \tag{4.3}$$

Identifying the energy dissipating components in (3.1) and (4.3), we obtain the ε value

$$\varepsilon = \frac{1}{\sqrt{\pi\beta}} = \frac{1}{\sqrt{\pi}}\frac{\sqrt{\nu T}}{D}. \tag{4.4}$$

In the laminar flow regime, with $\beta \simeq 40\,000$, we obtain $\varepsilon = 0.003$. As argued in § 3, the actual ε value is expected to be much larger.

Therefore the two values $\varepsilon = 0.003$ (laminar boundary layer) and $\varepsilon = 0.03$ (turbulent or nearly turbulent boundary layer) were selected for the calculations. The $\varepsilon = 0.03$ value was first chosen somewhat arbitrarily. As will appear in the next section, it turned out to provide results in good agreement with the measurements.

The boundary condition (4.1) was implemented in the potential flow model. It was imposed at the vertical walls of the cylinders, while the usual no-flow condition was kept at the bottom. In Kagemoto & Yue's interaction theory, the fluid domain around each cylinder is divided into two regions: an inner subdomain below the cylinder and an outer domain, where the scattered velocity potential is expressed as:

$$\phi_i^S(r_i, \theta_i, z) = \frac{\cosh k_0(z + h)}{\cosh k_0 h} \sum_{n=-\infty}^{\infty} A_{0n_i} H_n(k_0 r_i) \exp(\mathrm{i}n\theta_i) + \sum_{m=1}^{\infty} \cos k_m(z + h) \sum_{n=-\infty}^{\infty} A_{mn_i} K_n(k_m r_i) \exp(\mathrm{i}n\theta_i), \tag{4.5}$$

where (r_i, θ_i, z) is the cylindrical coordinate system fixed to the ith cylinder and H_n, K_n are the nth-order Hankel function of the first kind ($H_n = J_n + \mathrm{i}Y_n$) and modified Bessel function of the second kind, respectively. The water depth h is assumed to be constant, and k_0 and k_m are the wavenumbers of the progressive and evanescent modes, respectively. Implementing the boundary condition (4.1), rather than the usual no-flow condition at the wall $r_i = a$, merely results in a slight modification of the linear systems that relate the A_{mni} coefficients.

For validation, the same development was performed in the quasi-analytical model

due to Linton & Evans (1990). This model applies to cylinders standing on the sea-floor. The diffraction potential ϕ_D is expressed as

$$\phi_D = \frac{\cosh k_0(z+h)}{\cosh k_0 h} \sum_{i=1}^{N_c} \sum_{m=-\infty}^{\infty} A_m^i Z_{m0}^i H_m(k_0 r_i) \exp(\mathrm{i}m\theta_i), \tag{4.6}$$

where $Z_{m0}^i = J_m'(k_0 a_i)/H_m'(k_0 a_i)$.

The use of Graff's theorem for Bessel functions permits us to enforce the boundary condition (4.1) on each cylinder. The interaction coefficients A_m^i are found to verify the linear system of equations:

$$A_m^i \left[1 + \mathrm{i}\frac{\varepsilon}{k_0 a_i}\frac{H_m(k_0 a_i)}{H_m'(k_0 a_i)}\right] + \sum_{j\neq i}^{N_c} \sum_{n=-\infty}^{\infty} A_n^j Z_{n0}^j \exp(\mathrm{i}(n-m)\alpha_{ji}) H_{n-m}(k_0 R_{ji}) \left[1 + \mathrm{i}\frac{\varepsilon}{k_0 a_i}\frac{J_m(k_0 a_i)}{J_m'(k_0 a_i)}\right] = -I_i \exp(\mathrm{i}m(\pi/2-\beta)) \left[1 + \mathrm{i}\frac{\varepsilon}{k_0 a_i}\frac{J_m(k_0 a_i)}{J_m'(k_0 a_i)}\right], \tag{4.7}$$

where $I_i = \exp(\mathrm{i}k_0[X_i \cos\beta + Y_i \sin\beta])$ is the phase correction accounting for the position (X_i, Y_i) of each of N_c cylinders and β is the incident angle of the incoming wave.

In figures 5(a) and 5(b) we present comparative results obtained with the two numerical models. Both figures show the RAO of the free-surface elevation, between cylinders 6 and 7 of the 50 cylinder array, versus the wave period which ranges from 0.67 to 0.75 s. With the Linton & Evans method the cylinders are assumed to be bottom-seated (at a waterdepth of 2.2 m), whereas with the Kagemoto & Yue method, calculations are performed at draughts of 0.645 m (more than half the maximum wavelength) and 0.215 m (the draught of the tested cylinders). In figure 5(a), the ε coefficient is set equal to zero (no energy dissipation), while in figure 5(b) it is equal to 0.03. It can be observed that the Linton & Evans method (bottom-seated cylinders) and the numerical model at 0.645 m draught provide identical results, within graphical accuracy, both for $\varepsilon = 0$ and $\varepsilon = 0.03$. This agreement validates the modifications performed in the codes. For the 0.215 m draught cylinders, a small shift toward the lower periods can be observed. This shift is of about 0.002 s at wave periods around 0.7 s.

This decrease of the resonant period is in qualitative agreement with the results obtained by Linton & Evans (1992) who derive the trapped mode frequencies for vertical truncated cylinders at the centreline of a channel. For the same a/d value of 0.5, they find (see their table 1) that, at a draught to radius ratio D/a of 2, the resonant $k_0 d$ value is 1.41, while at D/a ratios of 4 and 5, it is equal to 1.39, that is the same value as for a bottom-standing cylinder. In our experiments, the draught to radius ratio is 2.6 and the -0.002 s shift means a resonant $k_0 d$ value slightly below 1.40.

5. Comparison with experimental results

Figures 6(a)–6(e), corresponding to figures 2(c)–2(g), show the newly calculated free-surface elevations along the array, for wave periods of 0.68, 0.69, 0.70, 0.71 and 0.72 s. In figure 6(a), relating to a wave period of 0.68 s, below the resonant range,

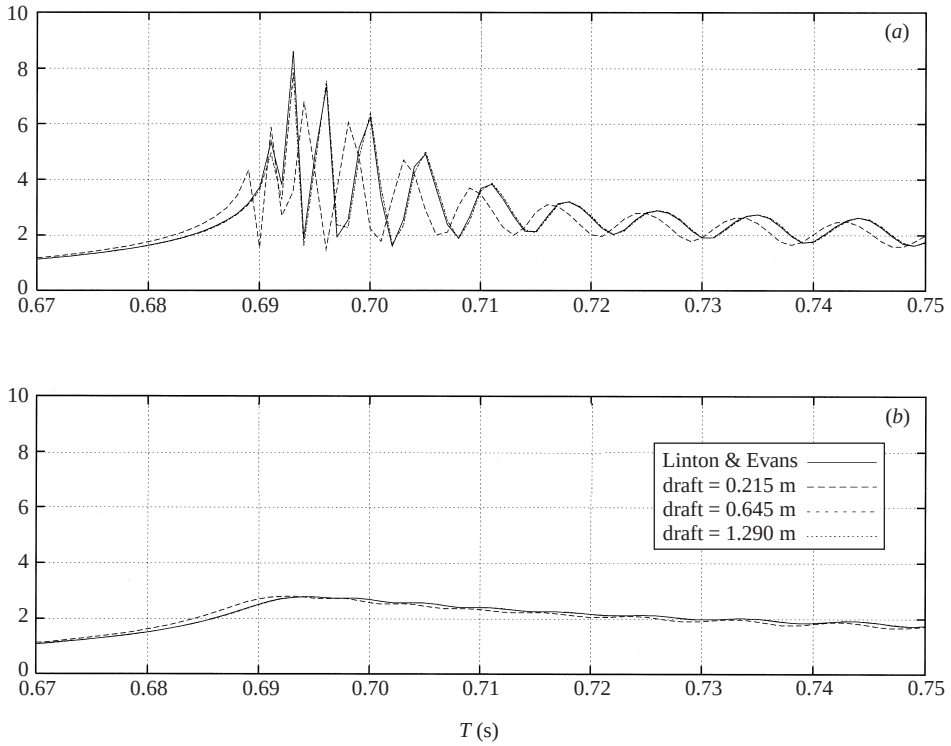

FIGURE 5. Calculated values of the RAOs of the free-surface motion, between cylinders 6 and 7, *vs.* the wave period, for different drafts of the cylinders. (*a*) No energy dissipation. (*b*) With energy dissipation ($\varepsilon = 0.03$).

nearly identical numerical results are obtained whatever the ε value. Results for lower wave periods are not shown, but the same conclusion was reached: energy dissipation plays a negligible role at these wave periods and the rapid decay along the array is due to diffraction effects. In the subsequent figures, relating to the resonant range, the numerical results appear to be quite sensitive to the ε value. With the larger ε value of 0.03, the agreement with the measured values is quite good. (The experimental results shown in the figures are those referred to as '1st' in figures 2*c*–2*g*). In figure 6(*b*), relating to the resonant period of 0.69 s, we present numerical results for other ε values, that is 0.01, 0.02 and 0.04. It can be observed that numerical results at ε values less than 0.02 are far off the experimental results, while the $\varepsilon = 0.03$ and $\varepsilon = 0.04$ are quite close. These results confirm our choice of $\varepsilon = 0.03$, as a minimum value to represent energy dissipation in the boundary layers.

It can also be noted in the figures that the viscous attenuation is stronger in the lee part of the array, as the waves lose energy while they travel along. As a result, attenuation is also observed when the wave period is far beyond the resonant range, as is shown in the following section.

As predicted by Maniar & Newman (1997), another type of trapped mode, which they called the Dirichlet trapped mode, also occurs for the present array of 50 cylinders. For a radius to half-spacing a/d ratio of 0.5, and for 50 cylinders, it is predicted that it takes place at $k_0 d = 3.068774$ (their table 3), which corresponds to a wave period of 0.465 s in the present experiment. Figure 7 shows the calculated RAOs of the vertical motion of the free surface at the midpoint of the 5th cylinder and the 6th cylinder in the array of 50 cylinders. It is shown in Maniar & Newman (see

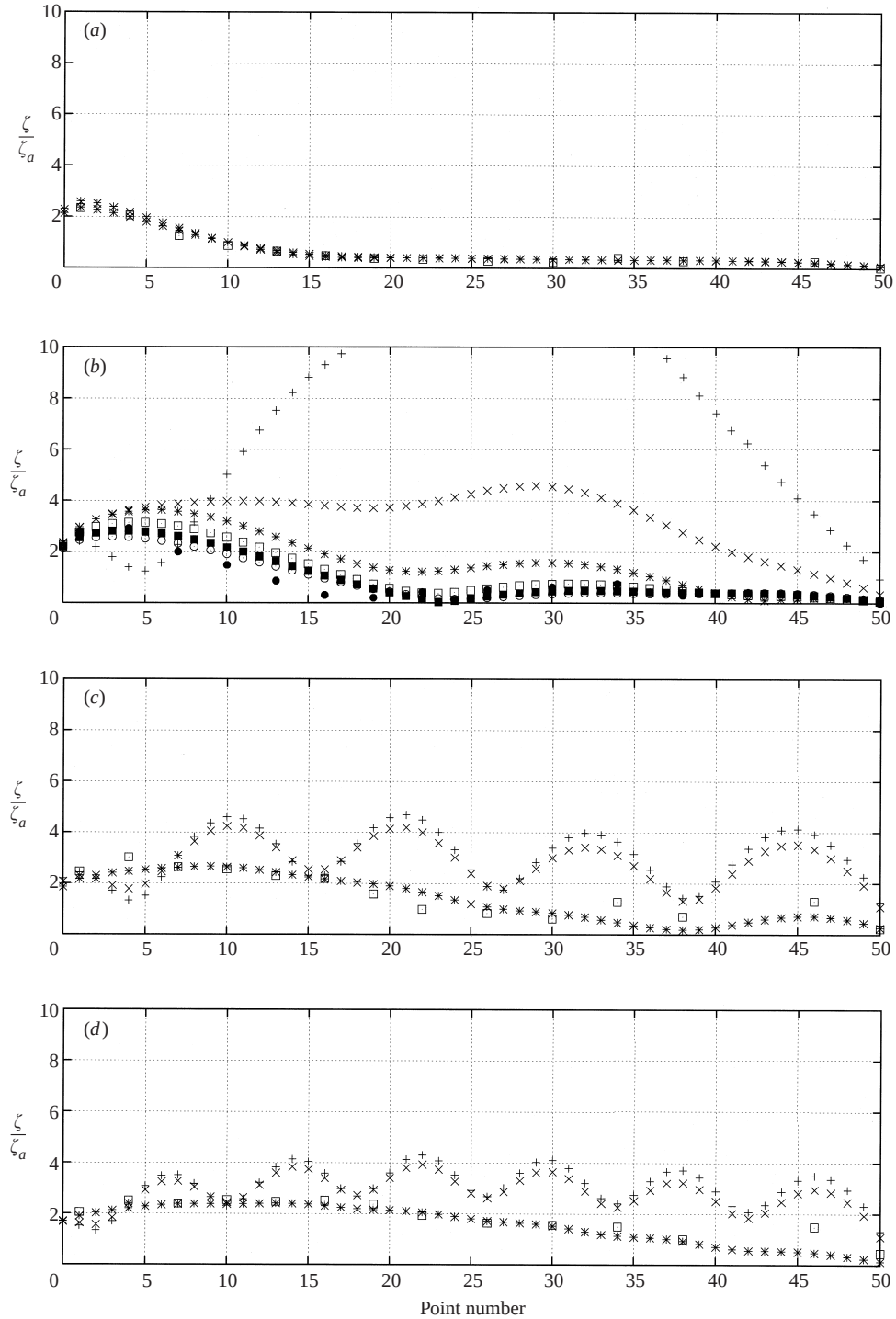

FIGURE 6. For caption see facing page.

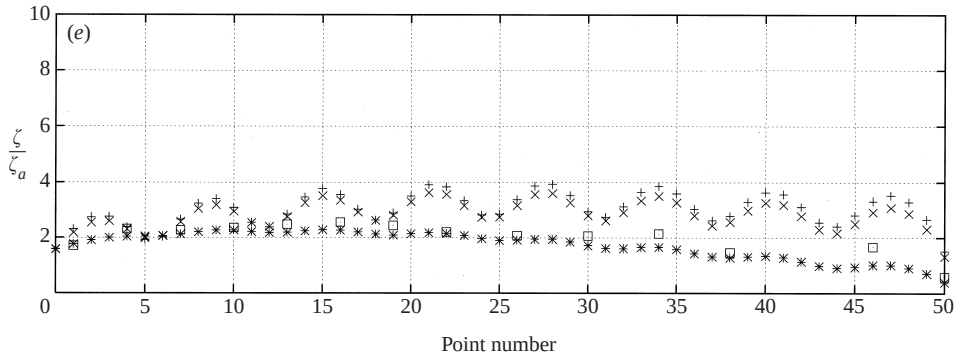

FIGURE 6. Response amplitude operators of the free-surface motion along the array. Measured *vs.* calculated values, with and without energy disspation. Wave period (*a*) 0.68 s; (*b*) 0.69 s (with additonal computations for $\varepsilon = 0.01, 0.02, 0.04$); (*c*) 0.70 s. (*d*) 0.71 s; (*e*) 0.72 s. (*a*), (*c*)–(*e*) +, $\varepsilon = 0$; ×, 0.003; ∗, 0.03; □, exp. (*b*) +, $\varepsilon = 0$; ×, 0.003; ∗, 0.01; □, 0.02; ■, 0.03; ○, 0.04; •, exp.

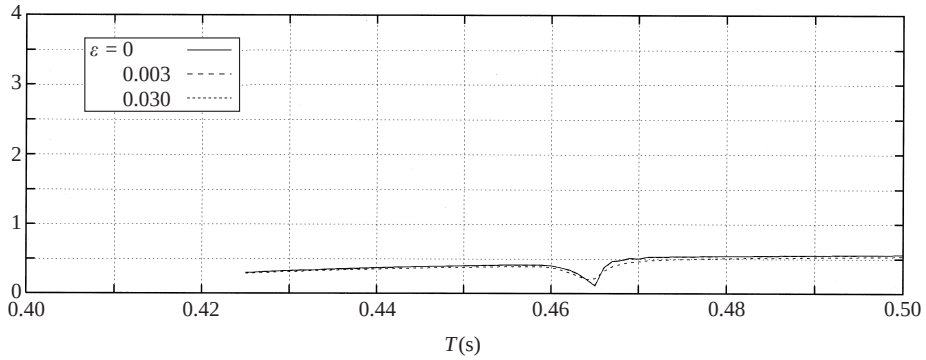

FIGURE 7. Calculated values of the RAOs of the free-surface motion, between cylinder 5 and 6 in the neighbourhood of the Dirichlet-trapped-mode wave period.

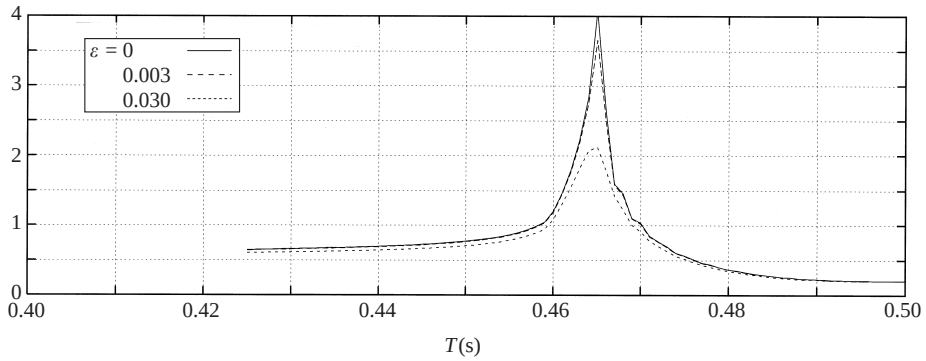

FIGURE 8. Calculated values of the RAOs of the free-surface motion along the lee-side surface of cylinder 5 in the neighbourhood of the Dirichlet-trapped-mode wave period.

their figure 4) that the vertical free-surface displacement is antisymmetric about the midpoint between adjacent cylinders when waves are trapped in the Dirichlet mode, which explains why the RAO curve in figure 7 displays the steep hollow at the wave period 0.465 s. On the other hand, the RAO of the vertical free-surface displacement

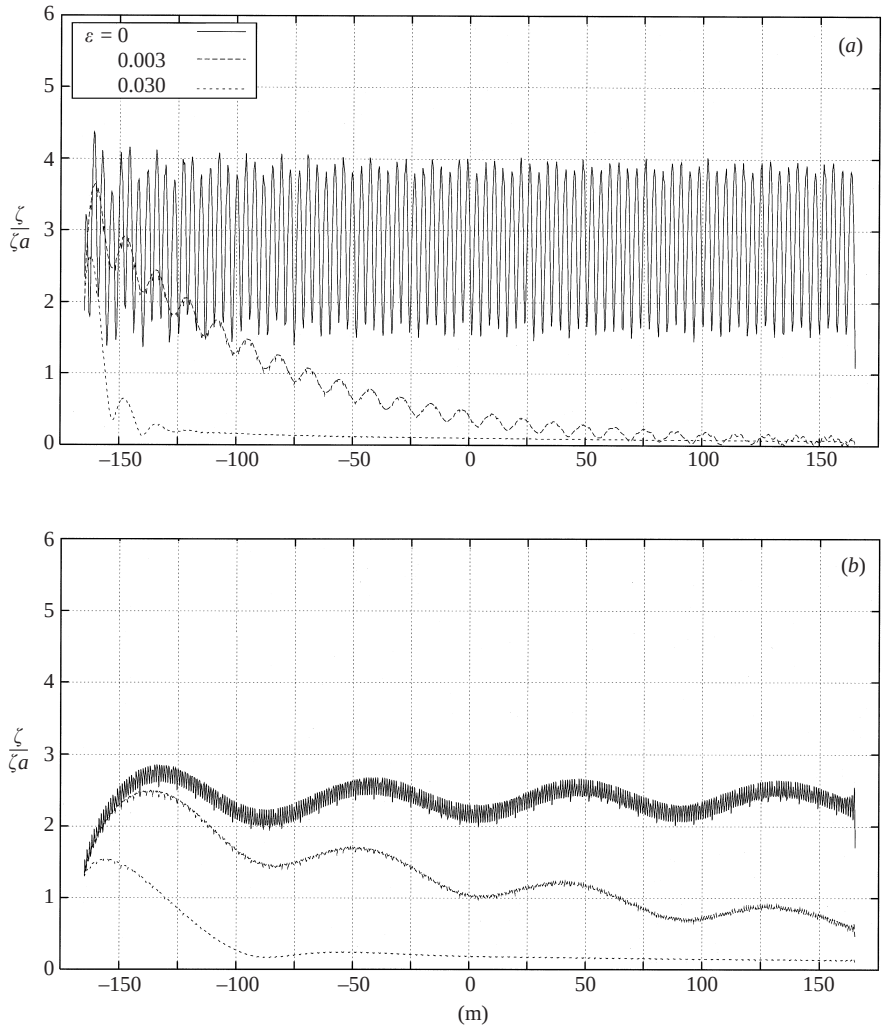

FIGURE 9. For caption see facing page.

increases sharply near the cylinder, as shown in figure 8, which depicts the RAOs of the vertical displacement of the free-surface at the (lee-side) wall of the 5th cylinder. With $\varepsilon = 0.03$, the peak RAO value is decreased from 4 to 2.

6. Application of the numerical model to arrays of extremely large numbers of legs

In this section we present results of calculations performed for geometries consisting of large numbers of identical truncated cylinders. First, a single array of 1000 cylinders is considered, then a rectangular arrangement of 16×80 cylinders, more representative of the legs supporting a floating airport. The spacings, diameters and draughts are the same as with the 50 cylinder array, except that for the 16×80 cylinder geometry, the draught is reduced to 0.11 m.

This practical application raises the question of the ε value to adopt in full scale. Assuming diameters around 5 m, wave periods of about 4 s, and an effective viscosity

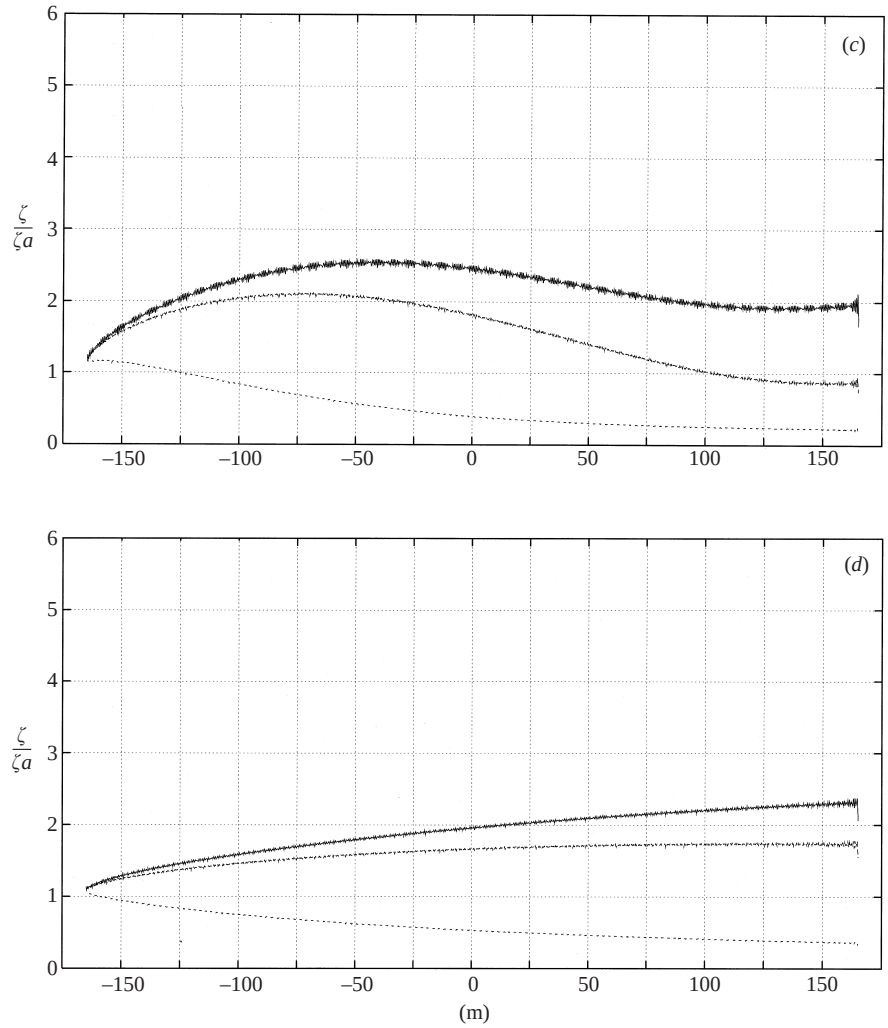

FIGURE 9. 1000 cylinder array. Calculated value of the free-surface motion along the array. Wave period (*a*) 0.70 s; (*b*) 0.80 s; (*c*) 0.90 s; (*d*) 1.0 s.

equal to 100 times the molecular viscosity, gives $\varepsilon = 0.002$ when applying equation (4.4). The dissipation of energy is much reduced, as compared to what is achieved at model scale. This is an issue that deserves further consideration.

6.1. *An array of 1000 cylinders*

Figure 9 gives the RAO of the free-surface elevation along the array (between adjacent cylinders), for wave periods of 0.70, 0.80, 0.90 and 1.0 s, and for the three ε values: 0, 0.003 and 0.03. With no energy dissipation, there is no decay of the free-surface motion along the array. At the largest wave period (1 s), we may even note that the RAO steadily increases. With the largest ε value, corresponding to model scale, a very quick decay can be observed at the lower wave periods (0.7 and 0.8 s). At 0.9 and 1 s the decay is less pronounced. At the intermediate ε value, more representative of full-scale arrays, the decay is much slower.

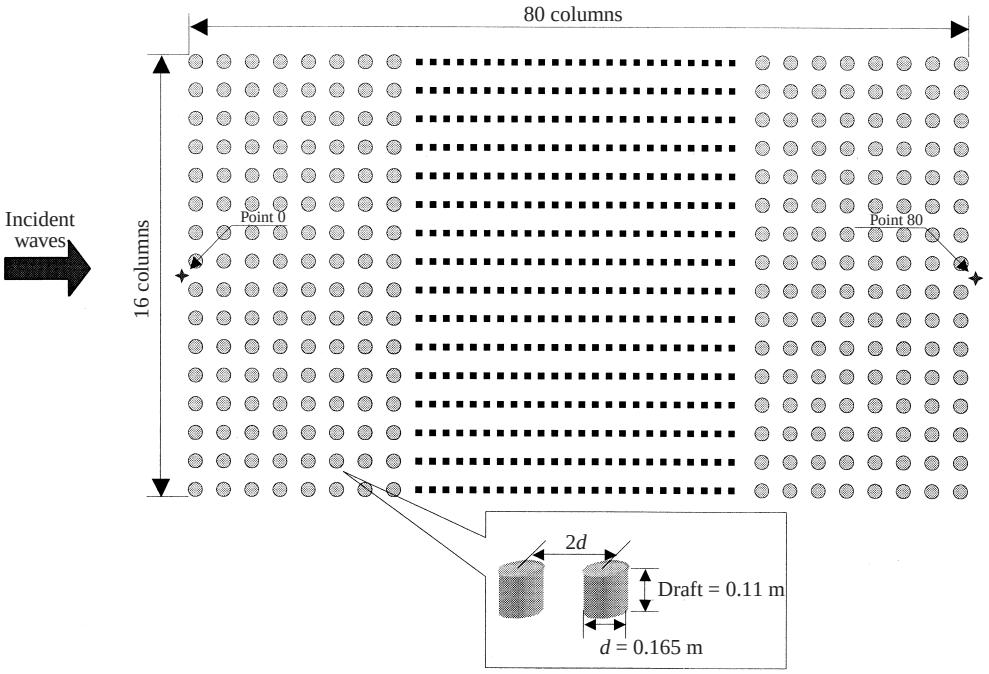

FIGURE 10. Geometry of an array of 16 × 80 cylinders.

6.2. *An array of 16 × 80 cylinders*

In order to see the effect of multiple rows, calculations were conducted for an array of 16 × 80 cylinders, in which 80 cylinders are arrayed in the longitudinal direction parallel to the incident-wave propagation while 16 cylinders are arrayed in the transverse direction, as shown in figure 10. The trapped mode analysis of N cylinders at the centreline of a channel was given by Evans & Porter (1997). They found that for N cylinders there are up to N trapped modes, with associated wavenumbers $k_0 d$ ranging from $\frac{1}{2}\pi$ down to much lower values than for the single-cylinder case. They do not provide results for 16 cylinders but, from their findings, we can expect resonant peaks to occur from a wave period of 0.65 s ($k_0 d = \frac{1}{2}\pi$) up to much larger values than in the single-row case.

This can be seen in figure 11 which shows the surface-displacement-amplitude characteristics versus the wave period at the two locations shown in figure 10 on the longitudinal centreline of the array. In figure 11(a), at the weather side, the calculated RAOs are hardly modified with $\varepsilon = 0.003$. With $\varepsilon = 0.03$, the smaller peaks of the response are filtered out. On the lee side (figure 11(b)), the free-surface motion is drastically reduced, all over the wave period range, at the larger value of ε. On the other hand, at $\varepsilon = 0.003$, the damping effect is much less pronounced.

If we infer that $\varepsilon \sim 0.003$ relates to the full-scale case and that $\varepsilon \sim 0.03$ relates to the model scale, we are led to conclude that model tests cannot be relied upon to study the wave interaction problem with multiple vertical cylinders.

7. Conclusions

An experimental study has been presented, on regular wave interaction with an array of 50 cylinders. In the wave period range of the Neumann trapped mode, much

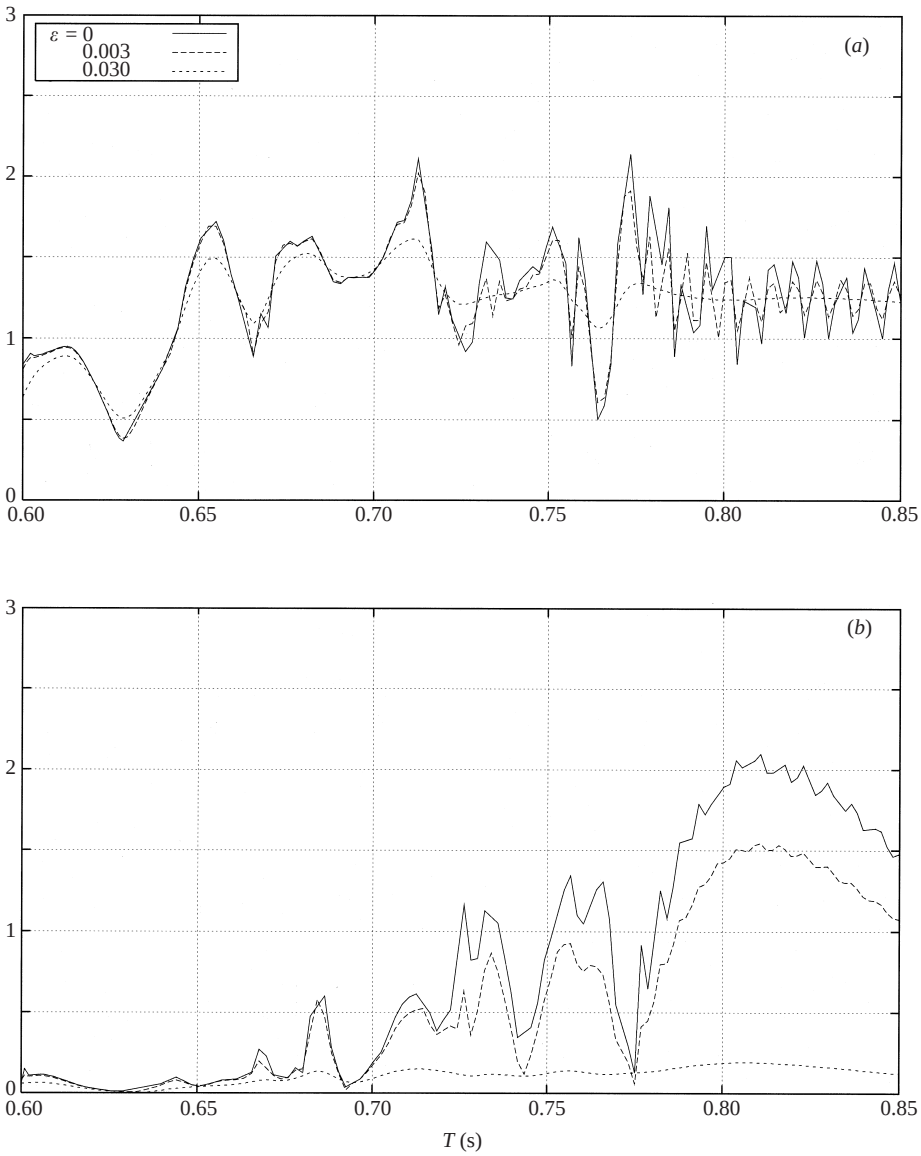

FIGURE 11. 16 × 80 cylinder array. Calculated values of the RAOs of the free-surface motion at (*a*) point 0; (*b*) point 80 (see figure 10).

less resonance has been observed than predicted by linearized potential flow theory. This damping phenomenon has been attributed to viscous dissipative effects taking place within the boundary layers at the cylinder walls. To reproduce these dissipative effects within the potential flow model, it has been suggested that we render the walls slightly porous, as is customary in harbour and coastal engineering. With this modification in the numerical codes, and an appropriate choice of the 'leakage coefficient' ε, very good agreement has been achieved with the experimental results.

Numerical results have also been given for wave periods outside the Neumann trapped mode range. At lower periods, viscous dissipation has no effect; the quick decay of the wave action along the array is due to diffraction effects, as noted

by Maniar & Newman (1997). At larger periods, potential flow models predict no attenuation, whatever the length of the array. When viscous dissipation has been introduced, it has been found that the wave action slowly decreases along the array, even for wave periods well above the critical range. These results have been confirmed by calculations performed in the case of a very long array, composed of 1000 cylinders, and for a rectangular system composed of 16×80 cylinders. This latter geometry has some relevance to the projects of multi-column supported floating airports, that are considered in Japan.

This practical application raises the problem of the leakage coefficient ε to be used in full scale, when the Stokes parameter of the flow attains values as large as 5×10^6 and the Keulegan–Carpenter number is less than unity. Knowledge is lacking on this point. It is important to be able to find out the importance of scale effects for the experimental study of such structures.

For the particular geometry considered here of a truncated cylinder, it has been shown that the flow separation at its base induces negligible energy dissipation, as compared to what takes place within the boundary layers at the vertical walls. For smaller draught to diameter ratios, and/or in full scale (where the relative contribution of the boundary layers decrease), flow separation at the lower edges could become significant. An extension of the numerical model, to take this effect into account, would be to render the keel of the cylinder porous as well, and there to apply a quadratic discharge law. An iterative resolution method would have to be followed to solve the diffraction problem (e.g. see Molin 2001).

The authors acknowledge the constructive comments of the reviewers. They are grateful to Professor T. Sarpkaya for his assistance in the analysis of the energy dissipation in the boundary layers.

Preliminary results were given in the Proceedings and in the Discussions Report of the 14th International Workshop on Water Waves and Floating Bodies, held at Port-Huron, Michigan, in 1999 (R. F. Beck & W. W. Schultz editors).

Appendix. Energy dissipated through flow separation at the lower edges, as compared to the energy dissipated at the walls

In this Appendix we consider the case of one isolated truncated cylinder, submitted to a regular wave system, and we compare the energies dissipated through both processes.

We use results from experiments performed by Thiagarajan & Troesch (1994) who investigate the hydrodynamic heave damping of a vertical cylinder. Its diameter is 0.457 m and its draught 1.219 m. Forced heave motions are performed at a frequency (0.41 Hz) close to the heave natural frequency, resulting in very accurate measurements of the damping force, since the inertia and restoring forces nearly cancel each other. This damping force is partly due to friction at the vertical walls, and partly due to pressure forces induced by flow separation at the lower edges (as a result of the large draught , radiation damping is negligible). The friction component is linearly related to the heave velocity, while the pressure component is roughly proportional to the square of the heave velocity. By oscillating the model at varying amplitudes, the two contributions can be separated easily.

In Thiagarajan & Troesch's experiments, the β parameter, based on the diameter, is equal to 89 236. This is somewhat higher than the β value in our experiments, but the damping loads induced by flow separation should be little sensitive to the

Reynolds number, in so far as the edges are sharp. For K_C numbers in the range 0.2–1.0, Thiagarajan & Troesch find that this component of the damping force can be expressed as

$$F_s(t) = -\tfrac{1}{2}\rho C_D \pi a^2 \dot{Z}(t)|\dot{Z}(t)| \tag{A 1}$$

where $\dot{Z}(t)$ is the heave velocity and the drag coefficient C_D takes a value close to 1.5.

This is for a heaving cylinder in still water or, equivalently, for a fixed cylinder in uniform oscillatory flow (with a change in sign).

These results can be used in wave flows in so far as the wavelength is long as compared to the diameter, so that the incoming flow be nearly uniform at the cylinder bottom. In our experiments, it is not really the case (at 0.7 s period, the wavelength is about 4.5 times the diameter), but we shall nevertheless apply equation (A 1), with the vertical fluid velocity

$$W(t) = A\omega \exp(k_0 z_b) \sin \omega t. \tag{A 2}$$

Here, A is the free-surface motion amplitude and z_b is the vertical coordinate of the cylinder base, with respect to the still free surface. Then, the force due to flow separation takes the form

$$F_s(t) = \tfrac{1}{2}\rho C_D \pi a^2 A^2 \omega^2 \exp(2k_0 z_b) \sin \omega t |\sin \omega t|. \tag{A 3}$$

This can be expected to provide a good approximation of the actual force, even though the cylinder diameter is not really small when related to the wavelength.

The dissipated energy over a wave period is then

$$\Delta E_s = \int_0^T F_s(t) W(t)\, \mathrm{d}t = \tfrac{4}{3}\rho C_D \pi a^2 A^3 \omega^2 \exp(3k_0 z_b). \tag{A 4}$$

This dissipated energy is to be related to the one that takes place at the vertical walls of the cylinder, when they are made slightly porous and the boundary condition (4.1) is applied. The energy dissipated over a wave period is given by

$$\Delta E_w = \int_0^T \mathrm{d}t \iint_{S_w} \rho \frac{\partial \Phi}{\partial t} \frac{\partial \Phi}{\partial R}\, \mathrm{d}S = \rho \pi \frac{\varepsilon}{a} \iint_{S_w} \phi \phi^*\, \mathrm{d}S. \tag{A 5}$$

At the low wave periods of interest ($T \sim 0.7$ s), the wave action is quite diminished at the cylinder bottom. A good approximation can therefore be obtained by considering the case of an infinite draught cylinder, for which the velocity potential at the walls takes the simple form (e.g. see Mei 1983, chap. 7.5):

$$\phi = \frac{Ag}{\omega} \exp(k_0 z) \sum_{m=0}^{\infty} \frac{2\epsilon_m \mathrm{i}^{m+1}}{\pi k_0 a H_m'(k_0 a)} \cos m\theta. \tag{A 6}$$

where $\epsilon_m = 1$ for $m = 0$ and $\epsilon_m = 2$ for $m \geqslant 1$.

This is for a solid cylinder. It is the leading-order term for a slightly porous cylinder. The dissipated energy over a wave period is then

$$\Delta E_w = 4\rho \varepsilon \frac{A^2 g}{k_0^4 a^2} \sum_{m=0}^{\infty} \frac{\epsilon_m}{J_m'^2(k_0 a) + Y_m'^2(k_0 a)}. \tag{A 7}$$

Writing the two dissipated energies in non-dimensional form, we obtain:

due to flow separation:

$$\frac{\Delta E_s}{\rho\pi a^2 A^2 g} = \tfrac{4}{3} C_D k_0 A \exp(3k_0 z_b), \tag{A 8}$$

due to the leakage through the porous walls:

$$\frac{\Delta E_w}{\rho\pi a^2 A^2 g} = \frac{4\varepsilon}{\pi k_0^4 a^4} \sum_{m=0}^{\infty} \frac{\epsilon_m}{J_m'^2(k_0 a) + Y_m'^2(k_0 a)}. \tag{A 9}$$

At a 0.7 s wave period, the wavenumber k_0 is equal to $8.21\,\mathrm{m}^{-1}$. With $z_b = -0.215\,\mathrm{m}$ and $a = 0.0825\,\mathrm{m}$, keeping A and ε as variables, we obtain:
due to flow separation:

$$\frac{\Delta E_s}{\rho\pi a^2 A^2 g} = 0.082A, \qquad (A \text{ in m}) \tag{A 10}$$

due to the leakage through the porous walls:

$$\frac{\Delta E_w}{\rho\pi a^2 A^2 g} = 9.80\varepsilon. \tag{A 11}$$

Taking for A the maximum local value obtained experimentally $A \sim 0.05\,\mathrm{m}$, and $\varepsilon = 0.03$ (turbulent or nearly turbulent boundary layer), we find that ΔE_s is less than 1.5% of ΔE_w. So the energy dissipated through flow separation at the lower edges is negligible, as compared to the energy dissipated in the boundary layers at the vertical walls.

REFERENCES

Bearman, P. W., Downie, M. J., Graham, J. M. R. & Obasaju, E. D. 1985 Forces on cylinders in viscous oscillatory flow at low Keulegan–Carpenter numbers. *J. Fluid Mech.* **154**, 337–356.

Bearman, P. W. & Russell, M. P. 1996 Measurements of hydrodynamic damping of bluff bodies with application to the prediction of viscous damping of TLP hulls. In *Proc. 21st Symp. Naval Hydrodynamics, Trondheim, Norway*. National Academy Press.

Callan, M., Linton, C. & Evans, D. V. 1991 Trapped modes in two-dimensional wave guides. *J. Fluid Mech.* **229**, 51–64.

Evans, D. V. & Porter, R. 1997 Trapped modes about multiple cylinders in a channel. *J. Fluid Mech.* **339**, 331–356.

Hall, P. 1984 On the stability of unsteady boundary layer on a cylinder oscillating transversely in viscous fluid. *J. Fluid Mech.* **146**, 347–367.

Honji, H. 1981 Streaked flow around an oscillating circular cylinder. *J. Fluid Mech.* **107**, 509–520.

Kagemoto, H., Murai, M. & Saito, M. 1998 Wave decay characteristics along a long array of cylindrical legs. In *Proc. 13th Intl Workshop on Water Waves and Floating Bodies* (ed. A. J. Hermans), pp. 55–58.

Kagemoto, H. & Yue, D. K. P. 1986 Interactions among multiple three-dimensional bodies in water waves: an exact algebraic method. *J. Fluid Mech.* **166**, 189–209.

Linton, C. M. & Evans, D. V. 1990 The interaction of waves with arrays of vertical circular cylinders. *J. Fluid Mech.* **215**, 549–569.

Linton, C. M. & Evans, D. V. 1992 The radiation and scattering of surface waves by a vertical cylinder in a channel. *Phil. Trans. R. Soc. Lond.* A **338**, 325–357.

Maniar, H. D. & Newman, J. N. 1997 Wave diffraction by a long array of cylinders. *J. Fluid Mech.* **339**, 309–330.

Mei, C. C. 1983 The Applied Dynamics of Ocean Surface Waves. Wiley-Interscience.

Molin, B. 2001 Numerical and physical tanks: making them fit. *Ship Technol. Res.* **48**, 1–21.

Murai, M., Kagemoto, H. & Fujino, M. 2000 On the hydroelastic responses of a very large floating structure in waves. *J. Mar. Sci. Technol.* **4**, 123–153.

NEWMAN, J. N. 1997 Resonant diffraction problems. (Abstracts submitted to Georg Weinblum Special Meeting Lectures.) In *Proc. 12th Intl Workshop on Water Waves and Floating Bodies* (ed. B. Molin), pp. 307–308.

SARPKAYA, T. 1993 Coherent structures in oscillatory boundary layers. *J. Fluid Mech.* **253**, 105–140.

SARPKAYA, T. 1986 Force on circular cylinder in viscous oscillatory flow at low Keulegan–Carpenter number. *J. Fluid Mech.* **165**, 61–71.

STOKES, G. G. 1851 On the effect of the internal friction of fluids on the motion of pendulums. *Trans. Camb. Phil. Soc.* **9**, 8–106.

THIAGARAJAN, K. P. & TROESCH, A. W. 1994 Hydrodynamic heave damping estimation and scaling for tension leg platforms. *Trans. ASME* **116**, 70–76.

TROESCH, A. W. & KIM, S. K. 1991 Hydrodynamic forces acting on cylinders oscillating at small amplitudes. *J. Fluids Struct.* **5**, 113–126.

WANG, C.-Y. 1968 On high-frequency oscillating viscous flows. *J. Fluid Mech.* **32**, 55–68.